Doppler Signature Analysis of Perturbed Target Motion in Over-The-Horizon Radar

Yimin D. Zhang
Department of Electrical and Computer Engineering
Temple University
Philadelphia, PA 19122, USA

Braham Himed
Distributed RF Sensing Branch
Air Force Research Laboratory
WPAFB, OH 45433, USA

***Abstract*—Target geo-location is an important task in over-the-horizon radar. A useful approach is based on the Doppler signatures of the micro-multipath signals which reveal target motion and enable target state estimation. Target Doppler signatures, however, are sensitive to irregular target motions, thereby complicating the Doppler signature analyses. In this paper, we consider the Doppler signatures of micro-multipath signals for a target that moves with a constant altitude but its azimuth velocity and altitude are perturbed. We analyze the effect of such velocity and altitude variations in the resulting Doppler signatures. The Doppler frequency difference is estimated using the self-stationarized signals.**

Keywords: Doppler analysis, radar signal processing, over-the-horizon radar, target localization, short-time Fourier transform.

I. Introduction

Sky-wave over-the-horizon radar (OTHR) performs long-range surveillance beyond the limit of the earth horizon and thus provides valuable early-warning information [1–5]. Because the operation of OTHR systems highly depends on the ionospheric conditions which involve complicated propagation models and dynamically vary, accurate target geo-location is a challenging problem [6–9]. A promising approach is through the exploitation of time-frequency analysis of the time-varying Doppler signatures of the micro-multipath signals which has resulted in estimation and tracking methods for target velocities and altitude [10–16]. For a maneuvering target, the Doppler signatures of the micro-multipath signals reveals the azimuth (range-direction) and elevation motions of the target. More specifically, the nominal Doppler frequency reflects the target azimuth velocity, whereas the Doppler frequency difference between the different Doppler signature components is primarily associated with the target elevation velocity. As such, resolved time-frequency analysis of the micro-Doppler signatures enables effective estimation and tracking of target elevation velocity and altitude.

Such approaches have recently been applied to targets maintaining a constant altitude and moving with a constant velocity. In this case, the micro-Doppler frequencies exhibit parallel linear frequency modulated (LFM, also known as chirp) signatures with a small chirp rate that can effectively be analyzed using the fractional Fourier transform [17–20]. When such a target experiences velocity perturbations due to flight dynamics and the external atmospheric environment [21–23], the micro-multipath Doppler signatures of the target may deviate from the parallel LFM Doppler signal model. Such perturbations are associated with the aerodynamics which differ with target type and size, and are characterized by the unique dynamic parameters of each target. Therefore, while such perturbations complicate the Doppler signature analysis and estimation, careful examination of such perturbations has also revealed additional information about the targets for enhanced target recognition and classification.

Recently, the effect of perturbed target azimuth velocity and target altitude was considered separately in [24] and [25]. Target altitude perturbation mainly affects the Doppler difference between the micro-Doppler signatures. Under mild conditions, the fractional Fourier transform can still be applied to analyze the Doppler signatures, but performance degrades as the perturbation becomes severe. On the other hand, azimuth velocity variations cause the Doppler signatures of all micro-multipath components to be similarly affected. In this case, performing self-stationarization [26] removes the effect of azimuth velocity perturbation and converts the Doppler signatures into constant frequency components which can be conveniently analyzed using the Fourier transform or sparsity-based spectrum analysis methods.

In this paper, we consider the Doppler signatures of micro-multipath signals for a flying target that experiences perturbation in both the azimuth velocity and the target altitude. Exploiting the existing results reported in [24] and [25], we perform self-stationarization to remove the effect of azimuth velocity perturbation. The short-time Fourier transform is then applied to analyze the stationarized Doppler signals and estimate the Doppler frequency difference between the micro-multipath signals. It is noted that, unlike [24], which does analyze the time-variation of the micro-multipath Doppler frequencies due to target altitude variation, such time variation is examined in this paper through the consideration of the spectrogram.

II. Signal Model

We consider an OTHR system operated in a pseudo-monostatic mode, and where a target of interest flies with a constant azimuth velocity and at a fixed altitude. However, the actual target azimuth velocity and altitude are perturbed. The problem is considered in a simplified flat-earth model [11] as shown in Fig. 1, where H is the height of the ionosphere layer which is assumed to be constant and a coarse estimate is available from ionosonde monitoring, and h is an unknown target altitude to be estimated. Note in this figure that the targets and propagation paths showing below the ionosphere layer are physically present, whereas those above the ionosphere layer are their images due to ionosphere and ground reflections and are included in the figure for convenience of

The work of Y. D. Zhang is supported in part by a contract with Altamira Technologies Corp. for research sponsored by the Air Force Research Laboratory under Contract FA8650-18-C-1055.

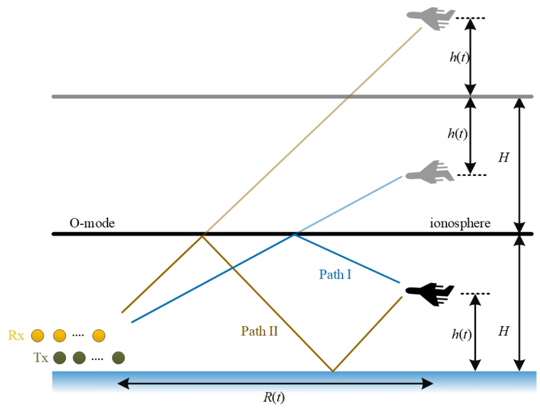

Fig. 1: Flat-earth local multipath propagation model of OTHR.

slant-range calculation.

The OTHR signals reflected by the target and observed at the radar receivers follow multiple round-trip paths due to their reflections from the ionosphere and the earth surface [10, 11]. As illustrated in Fig. 1, the specular earth surface and ionosphere reflections result in two different propagation paths for each of the transmit and receive OTHR signals. The one-way target range R_t is time-varying with velocity v_t, i.e.,

$$R_t = R_0 + \int_0^t v_t \mathrm{d}t. \tag{1}$$

The one-way slant ranges $l_t^{(1)}$ and $l_t^{(2)}$ of Path I and Path II are respectively obtained as [11]

$$l_t^{(1)} = \left(R_t^2 + (2H-h)^2\right)^{\frac{1}{2}} \approx R_t + \frac{2H}{R_t}(H-h), \tag{2a}$$

$$l_t^{(2)} = \left(R_t^2 + (2H+h)^2\right)^{\frac{1}{2}} \approx R_t + \frac{2H}{R_t}(H+h), \tag{2b}$$

where the approximations are obtained as first-order Taylor series expansion under the condition that $R_t \gg H \gg h$.

The combination of the two distinct paths for signal transmission and reception results in three distinct round-trip paths. For the first round-trip path, both transmit and receive signals propagate along Path I, denoted as $[l_1, l_1]$. Similarly, the second round-trip path $[l_2, l_2]$ follows Path II for both ways. The third round-trip path uses different forward and return paths, i.e., $[l_1, l_2]$ and $[l_2, l_1]$. The slant ranges of the three round-trip paths are respectively expressed as

$$L_t^{(1)} = 2l_t^{(1)}, \quad L_t^{(2)} = 2l_t^{(2)}, \quad L_t^{(3)} = l_t^{(1)} + l_t^{(2)}, \tag{3}$$

and their corresponding Doppler signatures are given as

$$\nu_t^{(i)} = -\frac{f_c}{c}\frac{\mathrm{d}L_t^{(i)}}{\mathrm{d}t} = -\frac{\mathrm{d}L_t^{(i)}}{\lambda\,\mathrm{d}t}, \qquad i = 1, 2, 3, \tag{4}$$

where f_c is the carrier frequency of the OTHR signal, c is the velocity of the electromagnetic wave, and $\lambda = c/f_c$ denotes the signal wavelength.

III. Target Doppler Characteristics

In this section, we first show the micro-multipath Doppler frequencies of a target in the baseline case, i.e., it flies with a constant velocity and maintains a fixed altitude. The effects of azimuth velocity and altitude perturbations are then described.

A. Doppler Signature in the Baseline Case

We consider the case that the target flies at a constant velocity $\dot{R} = v_0$, and its altitude is fixed as h. In this case, using the results given in Eq. (2), the derivatives of the one-way slant ranges are expressed as

$$\frac{\mathrm{d}l_t^{(1)}}{\mathrm{d}t} \approx \dot{R} - \frac{2H\dot{R}}{R_t^2}(H-h), \quad \frac{\mathrm{d}l_t^{(2)}}{\mathrm{d}t} \approx \dot{R} - \frac{2H\dot{R}}{R_t^2}(H+h). \tag{5}$$

The Doppler frequencies of the three round-trip paths become

$$\nu_t^{(1)} = \bar{\nu}_t + \Delta\nu_t, \quad \nu_t^{(2)} = \bar{\nu}_t - \Delta\nu_t, \quad \nu_t^{(3)} = \bar{\nu}_t, \tag{6}$$

where

$$\begin{aligned}\bar{\nu}_t &= -\frac{\mathrm{d}(l_t^{(1)} + l_t^{(2)})}{\lambda \mathrm{d}t} \approx -\frac{2}{\lambda}\dot{R} + \frac{4H^2}{\lambda R_t^2}\dot{R} \\ &\approx -\frac{2}{\lambda}\dot{R} + \frac{4H^2}{\lambda R_0^2}\dot{R} - \frac{8H^2}{\lambda R_0^3}\dot{R}^2 t\end{aligned} \tag{7}$$

is termed as the nominal Doppler frequency, and

$$\Delta\nu_t = -\frac{\mathrm{d}(l_t^{(1)} - l_t^{(2)})}{\lambda \mathrm{d}t} \approx \frac{4Hh}{\lambda R_t^2}\dot{R} \tag{8}$$

is referred to as the Doppler frequency difference between the micro-Doppler components. For constant values of $\dot{R}$ and h, the first two terms at the right-hand side of Eq. (7) contribute to a dominant but constant Doppler frequency which is proportional to the target azimuth velocity $\dot{R}$, and the right-hand side of Eq. (8) contributes to a Doppler frequency difference which is proportional to both $\dot{R}$ and the target altitude h. The last term of the right-hand side of Eq. (7) renders the nominal Doppler component as a slowly time-varying LFM with the chirp rate determined by $\dot{R}$.

When considering $\Delta\nu_t$ given in Eq. (8) and because the variation of R_t is very small, i.e., $|\dot{R}t| \ll R_0$, it can be approximated as a constant, i.e., $R_t \approx R_0$. Thus, we have

$$\Delta\nu_t \approx \frac{4Hh}{\lambda R_t^2}\dot{R} \approx \frac{4Hh}{\lambda R_0^2}\dot{R} := \Delta\nu. \tag{9}$$

Therefore, the three Doppler signatures are equi-distant LFM components separated by a constant Doppler frequency difference $\Delta\nu$. The Doppler signatures of the first and second round-trip paths are symmetric and wrap around that of the third round-trip path, which coincides with the nominal Doppler frequency $\bar{\nu}_t$.

B. Target with Time-Varying Constant Acceleration

When the constant azimuth velocity of a target is perturbed, the instantaneous Doppler signature will deviate from the parallel LFM model. Consider a general model in which the instantaneous target velocity is described as

$$\dot{R}_t = v_0 + \int_0^t a_t \mathrm{d}t := v_0 + \Delta\dot{R}_t, \tag{10}$$

where a_t is the instantaneous acceleration. In this case, the nominal Doppler frequency becomes

$$\begin{aligned}\bar{\nu}_t &\approx -\frac{2}{\lambda}\dot{R}_t + \frac{4H^2}{\lambda R_0^2}\dot{R}_t - \frac{8H^2}{\lambda R_0^3}\dot{R}_t^2 t \\ &= -\frac{2}{\lambda}(v_0 + \Delta\dot{R}_t) + \frac{4H^2}{\lambda R_0^2}(v_0 + \Delta\dot{R}_t) - \frac{8H^2}{\lambda R_0^3}(v_0 + \Delta\dot{R}_t)^2 t.\end{aligned} \tag{11}$$

Typical aircraft velocity fluctuations are much smaller than the aircraft velocity [23], that is, $|\Delta\dot{R}_t| \ll |v_0|$. Therefore, when $|a_t| \geq 4H^2 v_0^2/R_0^3$ holds, the chirp rate of the nominal Doppler frequency $\bar{\nu}_t$, that is, $\mathrm{d}\bar{\nu}_t/\mathrm{d}t$, is dominated by $-2a_t/\lambda$. As a result, the Doppler signatures depend on the perturbation patterns and will likely deviate from the LFM model described in Eq. (9).

On the other hand, the Doppler difference becomes

$$\Delta\nu_t \approx \frac{4Hh}{\lambda R_0^2}\dot{R}_t = \frac{4Hh}{\lambda R_0^2}(v_0 + \Delta\dot{R}_t) \approx \frac{4Hh}{\lambda R_0^2} v_0. \tag{12}$$

The last approximation is rendered from $|\Delta\dot{R}_t| \ll |v_0|$ as discussed above. It is clear that, when the target altitude h is perturbed, the Doppler frequency difference $\Delta\nu_t$ will vary proportionally. The impact of azimuth velocity perturbation on the Doppler frequency difference is insignificant.

These observations demonstrate that, when the target altitude is concerned, estimating the Doppler difference is much simpler than directly estimating the three Doppler signatures. The self-stationarization technique, which was introduced in [26], can be used to estimate the Doppler difference without taking into account the variation of the nominal Doppler frequency. Applying self-stationarization to the parallel Doppler signatures of the micro-multipath signals results in sinusoidal outputs which can be conveniently analyzed for the estimation of the difference Doppler frequency. The target altitude can be obtained from (12) using a coarse estimate of the target range and velocity.

IV. Doppler Signature Stationarization and Analysis

We describe the received signal in the following general form [26, 27]:

$$x_t = A^{(1)}\exp(j\phi_t^{(1)}) + A^{(2)}\exp(j\phi_t^{(2)}) + A^{(3)}\exp(j\phi_t^{(3)}), \tag{13}$$

where $A^{(i)}$ and $\phi_t^{(i)}$ are, respectively, the path gain and the instantaneous phase of the ith path for $i = 1, 2$, and 3. The instantaneous phases can be expressed as

$$\phi_t^{(i)} = -2\pi\int_0^t \nu_t^{(i)}\mathrm{d}t = -2\pi\int_0^t \left(\bar{\nu}_t + \xi^{(i)}\Delta\nu\right)\mathrm{d}t, \tag{14}$$

where $\xi^{(1)} = 1$, $\xi^{(2)} = -1$, and $\xi^{(3)} = 0$.

For clarity, we denote $\theta_t = -2\pi\int_0^t \bar{\nu}_t\mathrm{d}t$ and $\psi_t = -2\pi\int_0^t \Delta\nu\mathrm{d}t$ as the phase terms respectively corresponding to the nominal Doppler frequency and Doppler frequency difference. Then, Eq. (14) can be written as

$$\phi_t^{(1)} = \theta_t + \psi_t, \quad \phi_t^{(2)} = \theta_t - \psi_t, \quad \phi_t^{(3)} = \theta_t. \tag{15}$$

Signal self-stationarization is achieved by multiplying x_t with its conjugation, x_t^*, resulting in

$$\begin{aligned} |x_t|^2 = &\left(|A^{(1)}|^2 + |A^{(2)}|^2 + |A^{(3)}|^2\right) \\ &+ \left[A^{(1)}(A^{(3)})^* + (A^{(2)})^*A^{(3)}\right]\exp(-j\psi_t) \\ &+ \left[(A^{(1)})^*A^{(3)} + A^{(2)}(A^{(3)})^*\right]\exp(j\psi_t) \\ &+ A^{(1)}(A^{(2)})^*\exp(-j2\psi_t) + (A^{(1)})^*A^{(2)}\exp(j2\psi_t). \end{aligned} \tag{16}$$

TABLE I: Key Parameters

Parameter	Notation	Value
Initial range	R_0	2,500 km
Ionosphere height	H	350 km
Target altitude	h	20 km
Target initial velocity	v_0	-500 m/sec
Carrier frequency	f_c	16 MHz
Pulse repetition frequency	f_s	110 Hz
Signal-to-noise ratio	SNR	-5 dB
Coherent processing interval	T	80 s

It is clear from the above expression that the resulting product $|x_t|^2$ does not depend on θ_t. It contains a DC component as well as $\pm\psi_t$ and $\pm 2\psi_t$ terms. As a result, the effect in the nominal Doppler frequency variation due to the target azimuth velocity perturbation vanishes, thereby enabling robust estimation of the Doppler difference.

To provide improved visualization and estimation of the Doppler frequency difference, two post-processing steps are carried out. First, we remove the dominant DC component, which does not carry useful information related to the target Doppler signatures, through a simple subtraction of the signal average component. Second, we fuse the information contained in the harmonic non-zero frequency signatures to enhance the desired component of $\Delta\nu$. Denote $X(f)$ as the spectrum of $|x_t|^2$, we compute the following quantity:

$$Y(f) = |X(f)X(f/2)|. \tag{17}$$

Because the spectrum is symmetric, only the positive frequency needs to be considered. It is also noted that the nominal Doppler frequency removal through self-stationarization works for different azimuth velocity variation patterns [25].

V. Simulation Results

Consider a target flying at a constant altitude, and the other key radar parameters are listed in Table I. Note that the input signal-to-noise ratio (SNR) includes the array gain if the OTHR is operated using multiple antennas or a multiple-input multiple-output (MIMO) radar system. To show the effectiveness of the proposed method, we consider a scenario in which the target simultaneously experiences a sinusoidal height variation and a sinusoidal horizontal velocity variation. The maximum deviation of the altitude perturbation is 7 m and the period is 40 s, whereas the maximum deviation of the horizontal velocity is 5 m/s and the period is 80 s.

Fig. 2(a) shows the Doppler signatures of the three micro-multipath components which are almost parallel and vary sinusoidally because of the azimuth velocity perturbation. The effect of the target altitude perturbation is insignificant to be observed in this plot. In Fig. 2(b), we plot the Doppler frequency difference, $\Delta\nu_t$. The variation due to the target altitude perturbation can now clearly be seen. For reference, when the target does not suffer from altitude perturbation, the Doppler difference takes an approximately constant value of 0.108 Hz, and the approximate value obtained from Eq. (9) is 0.120 Hz. The difference is due to the fact that only the first-order Taylor series terms are considered in Eq. (9).

Fig. 3(a) shows the spectrogram of the Doppler frequencies of the micro-multipath signals corresponding to Fig. 2(a). A

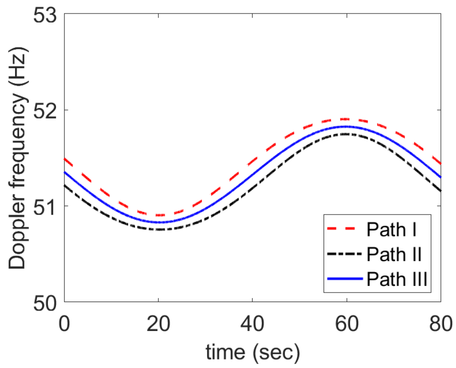

(a) Doppler frequencies of the micro-multipath signals

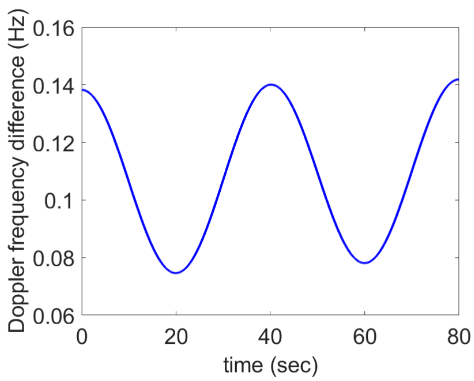

(b) Doppler frequency difference between the micro-multipath signals

Fig. 2: Doppler signatures of the three micro-multipath signals.

Hamming window of 2,047 samples (18.6 s) is used, and the number of frequency bins corresponding to the entire frequency span between -55 Hz and 55 Hz is $2^{13} = 8,192$. The spectrogram clearly shows the overall time-varying Doppler signatures which reflect the azimuth velocity perturbation. On the other hand, because of the time variation due to azimuth velocity perturbation and the small Doppler frequency difference, the individual Doppler signature of each multi-multipath component cannot be separably observed.

Fig. 3(b) shows the spectrogram of the micro-multipath signal after self-stationarization and DC removal. Only the positive frequency components are shown. A longer Hamming window of 4,095 samples (37.2 s) is used, and $2^{14} = 16,384$ frequency bins span the entire frequency range between -55 Hz and 55 Hz, rendering the frequency resolution to be 0.0067 Hz. Note that, because the Doppler difference is known to take a small value, we only need to compute the spectrogram corresponding to the frequency band of interest for reduced computation complexity. Fig. 3(c) shows the estimated Doppler frequency difference obtained from the spectrogram. While the peak Doppler frequency difference is slightly compromised due to the windowing effect in computing the spectrogram, the Doppler frequency difference is closely estimated, particularly for the center portion of the time span. The discrepancies in the beginning and ending time periods are due to the zero-padding effect and can be improved by using sliding windows.

For reference, Fig. 3(d) shows the spectrum of the stationarized signal using the Welch's method with a Hamming window size of 1,364 samples (12.4 s). Such a result ignores the time-variation of the Doppler frequency difference and only provides the overall spectrum. The average Doppler frequency difference is estimated from the peak position as 0.107 Hz, which is very close to the true value of 0.108 Hz that corresponds to the case without altitude perturbation.

VI. Conclusion

In this paper, we have analyzed the Doppler frequency characteristics of target signals in OTHR when both target azimuth velocity and altitude are perturbed. Noticing that the azimuth velocity variation changes the Doppler signatures of all micro-multipath components in a similar manner, the nominal Doppler frequency signature is analyzed using the spectrogram of the micro-multipath signals. Further, we apply the self-stationarization approach to remove the effect of azimuth velocity perturbation in the the Doppler signatures so that the Doppler frequency difference, which depends on the target altitude and varies with time over a much smaller range, can be estimated. It is noted that the Doppler frequency difference analysis in the proposed technique is insensitive to different patterns of the target azimuth velocity variation.

VII. References

[1] M. Headrick and M. I. Skolnik, "Over-the-horizon radar in the HF band," *Proc. IEEE*, vol. 62, no. 6, pp. 664–673, June 1974.

[2] Y. Zhang, G. J. Frazer, and M. G. Amin, "Concurrent operation of two over-the-horizon radars," *IEEE J. Sel. Topics Signal Process.*, vol. 1, no. 1, pp. 114–123, June 2007.

[3] G. J. Frazer, Y. Abramovich, B. A. Johnson, "Use of adaptive non-causal transmit beamforming in OTHR: Experimental results," in *Proc. Int. Conf. Radar*, Adelaide, Australia, Sept. 2008, pp. 311–316.

[4] J. M. Headrick and S. J. Anderson, "HF over-the-horizon radar," Chapter 20 in M. Skolnik (ed.), *Radar Handbook, 3rd Ed.* McGraw-Hill, 2008.

[5] G. A. Fabrizio, *High Frequency Over-the-Horizon Radar: Fundamental Principles, Signal Processing, and Practical Applications*. McGraw-Hill, 2013.

[6] M. Papazoglou and J. L. Krolik, "Matched-field estimation of aircraft altitude from multiple over-the-horizon radar revisits," *IEEE Trans. Signal Process.*, vol. 47, no. 4, pp. 966–976, April 1999.

[7] R. H. Anderson, S. Kraut, and J. L. Krolik, "Robust altitude estimation for over-the-horizon radar using a state-space multipath fading model," *IEEE Trans. Aerospace Electron. Syst.*, vol. 39, no. 1, pp. 192–201, Mar. 2003.

[8] M. Papazoglou and J. L. Krolik, "Estimation of aircraft altitude and altitude rate with over-the-horizon radar," in *Proc. IEEE Int. Conf. Acoust. Speech Signal Process.,*, Phoenix, AZ, March 1999, pp. 2103–2106.

[9] J. Praschifka, L. J. Durbridge and J. Lane, "Investigation of target altitude estimation in skywave OTH radar using a high-resolution ionospheric sounder," in *Proc. Intl. Radar Conf.*, Bordeaux, France, Oct. 2009, pp. 1–6.

[10] Y. D. Zhang, J. J. Zhang, M. G. Amin, and B. Himed, "Instantaneous altitude estimation of maneuvering targets in over-the-horizon radar exploiting multipath Doppler signatures," *EURASIP J. Adv. Signal Process.*, vol. 2013, no. 2013:100, pp. 1–13, May 2013.

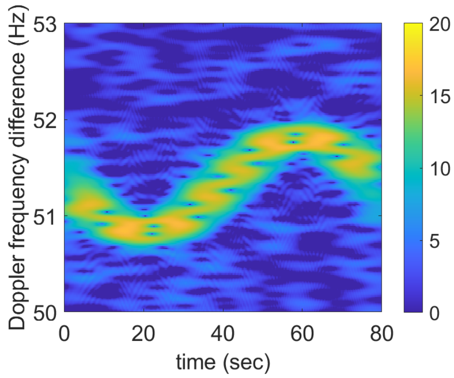

(a) Spectrogram of the Doppler signatures

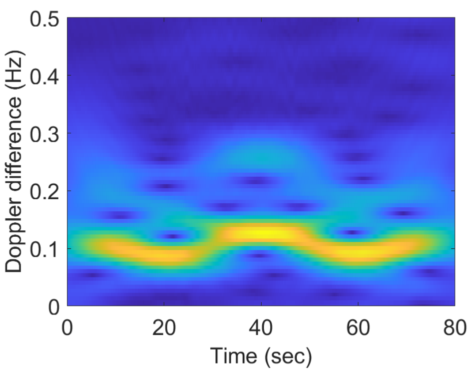

(b) Spectrogram of the stationarized Doppler signatures

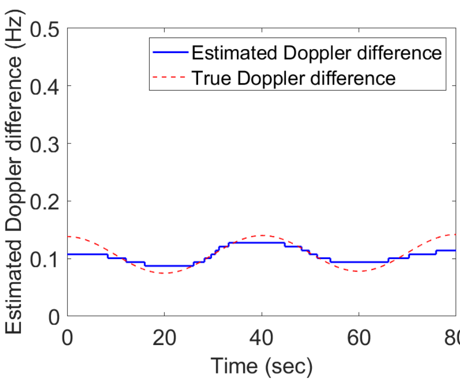

(c) Estimated Doppler frequency difference

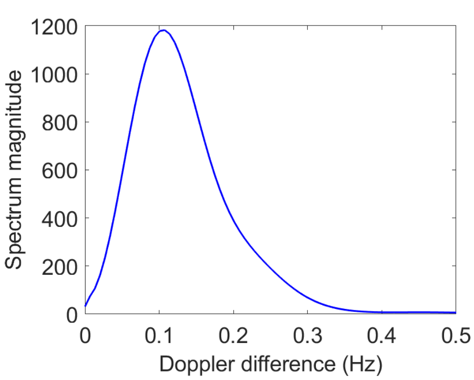

(d) Spectrum of stationarized signals

Fig. 3: Doppler signatures of the micro-multipath components (only the positive frequency range is shown for the Doppler frequency differences)

[11] Y. D. Zhang, M. G. Amin, and G. J. Frazer, "High-resolution time-frequency distributions for manoeuvring target detection in over-the-horizon radars," *IEE Proc.-Radar Sonar Navig.*, vol. 150, no. 4, pp. 299–304, Aug. 2003.

[12] C. Ioana, Y. D. Zhang, M. G. Amin, F. Ahmad, and B. Himed, "Time-frequency analysis of multipath Doppler signatures of maneuvering targets," in *Proc. IEEE Int. Conf. Acoust. Speech Signal Process.*, Kyoto, Japan, March 2012, pp. 3397-3400.

[13] C. Ioana, Y. D. Zhang, M. G. Amin, F. Ahmad, G. Frazer, and B. Himed, "Time-frequency characterization of micro-multipath signals in over-the-horizon radar," in *Proc. IEEE Radar Conf.*, Atlanta, GA, May 2012, pp. 671–675.

[14] Y. D. Zhang, M. G. Amin, and B. Himed, "Altitude estimation of maneuvering targets in MIMO over-the-horizon radar," in *Proc. IEEE Sensor Array Multich. Signal Process. Workshop*, Hoboken, NJ, June 2012, pp. 257–260.

[15] Y. D. Zhang, M. G. Amin, and B. Himed, "Direction-of-arrival estimation of nonstationary signals exploiting signal characteristics," in *Proc. Int. Conf. Inform. Science, Signal Process., and Their Appli.*, Montreal, Canada, July 2012, pp. 1223–1228.

[16] C. Hou, Y. Wang, and J. Chen, "Estimating target heights based on the earth curvature model and micro-multipath effect in skywave OTH radar," *J. Applied Math.*, vol. 2014, article ID 424191, pp. 1–14, 2014.

[17] A. Ahmed, Y. D. Zhang, and B. Himed, "Doppler signature analysis of mixed O/X-mode signals in over-the-horizon radar," in *Proc. IEEE Int. Radar Conf.*, Rockville, MD, April 2020, pp. 430–435.

[18] A. Ahmed, Y. D. Zhang, and B. Himed, "Doppler signature separation of mixed O/X-mode over-the-horizon radar signals," in *Proc. IEEE Radar Conf.*, Florence, Italy, Sep. 2020, pp. 1–5.

[19] Y. D. Zhang, A. Ahmed, and B. Himed, "Target altitude estimation in over-the-horizon radar," *IEEE Access*, vol. 10, pp. 11260–11273, Jan. 2022.

[20] A. Ahmed, Y. D. Zhang, and B. Himed, "Joint target and ionosphere parameter estimation in over-the-horizon radar," *IEEE Trans. Aerospace Electron. Syst.*, in press. doi: 10.1109/TAES.2022.3161396.

[21] B. Raghavan and N. Ananthkrishnan, "Small-perturbation analysis of airplane dynamics with dynamic stability derivatives redefined," in *AIAA Atmosph. Flight Mech. Conf. Exhibit*, San Francisco, CA, Aug. 2005, pp. 1–18.

[22] Y. Wang and B. Geerts, "Estimating the evaporative cooling bias of an airborne reverse flow thermometer," *J. Atmos. Oceanic Technol.*, vol. 26, no. 1, pp. 3–21, Jan. 2009.

[23] Brazil National Civil Aviation Agency, "Turbulence." Available at https://www.anac.gov.br/en/safety/aeronautical-meteorology/conditions/turbulence

[24] A. Ahmed, Y. D. Zhang, and B. Himed, "Doppler signature analysis of over-the-horizon radar signals with target altitude perturbation," in *Proc. IEEE Radar Conf.*, New York, NY, March 2022, pp. 1–6.

[25] Y. D. Zhang and B. Himed, "Doppler signature analysis in over-the-horizon radar for target with time-varying velocity," in *Proc. Int. Radar Symp.*, Gdańsk, Poland, Sept. 2022.

[26] Y. D. Zhang and B. Himed, "Multipath Doppler difference estimation in over-the-horizon radar," in *Proc. IEEE Radar Conf.*, Oklahoma City, OK, April 2018, pp. 693–697.

[27] V. S. Amin, Y. D. Zhang, and B. Himed, "Modified Viterbi-based local-multipath Doppler difference estimation in over-the-horizon radar," in *Proc. Asilomar Conf. Signals, Systems, and Computers*, Pacific Grove, CA, Nov. 2021, pp. 1612–1617.